

THE EFFECTS OF OXIDATION AND WEATHERING ON COAL COMBUSTION

S.L. Bend, I.A.S. Edwards and H. Marsh.
Northern Carbon Research Laboratories,
Dept. of Chemistry
University of Newcastle upon Tyne. NE1 7RU
United Kingdom

INTRODUCTION

General Review of Coal Oxidation

The low temperature oxidation of coal dramatically influences and alters inherent properties. The deleterious effect that oxidation has upon the coking and caking properties of coals, through the loss of plasticity and fluidity, is well documented [1,2,3]. The oxidative mechanism and processes by which coal properties are affected are discussed at length in the literature. Putnam *et al* [4], examining a suite of naturally weathered coals, discuss the possible transformation of aromatic compounds within the extractable organic material into molecules containing polar substituents. Larsen *et al* [2] suggest that the plasticity and fluidity of vitrinite rich coals can be lost by the oxidation of reactive benzylic positions and their replacement by carbonyl and carboxyl functional groups, with the concomitant loss of donatable hydrogen from the coal structure. In addition, an increase in cross-link density, due to the introduction of oxygen-bearing functional groups into the macromolecular structure of the coal, may prevent depolymerisation and plasticity during char formation.

Coal Oxidation Related to Combustion

Nandi *et al* [5], in their investigation into the role of inert coal macerals in pulverised fuel combustion, determined that the combustion efficiencies of coal were inversely related to the (organically) inert content of the coal feedstock during pilot-scale combustion experiments. Included in their category of organically inert material were what they considered to be oxidised vitrinite. Axelson *et al* [6], investigating the effects of oxidation upon in-situ outcroppings and stockpiled coal, discuss the problems encountered when attempting to characterise oxidised coal using conventional techniques, noting the additional complicating factors petrographic composition has upon techniques such as Free Swelling Index. They concur with earlier studies [2] that postulated different mechanisms for oxidation to occur above and below 80°C.

However, few studies discuss the effect that the oxidation of pulverised-coal feedstock has upon pyrolysis and combustion using Entrained Flow Reactor (EFR) apparatus. With increasing world coal trade that often requires the temporary stockpiling of coal, either prior to, or subsequent to, shipment to various points of usage, the effects of oxidation upon coal feedstock requires some attention. There are no grounds for assuming that the specifications quoted by the coal vendor or that the published characteristics of commercial steam coal are fixed and remain constant in time.

OBJECTIVES

The overall objective of this study is to investigate the effect of oxidation upon the pyrolysis and combustion of pulverised coal feedstock using laboratory based equipment. More specifically the study aims to:

1. Investigate the effect of artificial oxidation upon the intermediate char morphology of pulverised fuel.
2. Investigate the effect of natural weathering upon the intermediate char morphology of pulverised fuel.
3. Assess the suitability of existing coal characterisation techniques when seeking to determine the effects of oxidation upon coal feedstock.
4. Suggest new ways of characterising oxidised coal feedstock.

EXPERIMENTAL

Materials Used

The three freshly mined Carboniferous bituminous coals used in this study were supplied by British Coal and originate from coal mines within the Northumbrian coalfield (UK). Coal 88/024 and 88/026 are both British Coal (1964) class 500's, whereas coal 88/025 is a class 700 (steam raising coal). Their characteristics are given in Table 1.

Table 1. Some of the characteristics of the fresh coals used in this study

Coal	Rank (ASTM)	Ro max (%)	Maceral analyses (%)				Proximate analyses (wt %dry)	
			Vitrinite	Liptinite	Inertinite	Mineral Matter	V.M.	Ash.
88/025	Hvb B	0.73	61.2	14.4	23.8	0.6	39.0	4.8
88/026	Hvb A/B	0.79	76.4	12.2	11.6	0.0	35.0	10.02
88/024	Hvb A	0.93	72.2	12.4	14.8	0.6	37.0	5.1

Sample Preparation

The three freshly mined samples of coal were received in lump form ($>10 \text{ cm}^{-1}$) within hours of being mined. They were crushed to ($>2.5 \text{ mm}$) in a mechanical jaw crusher and each coal subdivided into twelve individual samples, representing two sets of six per coal. One set of five samples from each of the three coals was placed in a covered (lined) container and placed in the open air. The second set of five samples from each of the three coals was placed in a large heated receptacle and oxidised at 100°C (± 5) in static air. The sixth sample from each was analysed immediately and used as the datum sample. Samples of weathered and oxidised coal were removed periodically for analysis, thereby providing both artificially oxidised and 'weathered' samples.

Analytical Techniques

A Stanton Redcroft STA 780 TGA was used for all proximate analyses [7]. Calorific value determinations were obtained using a Gallenkamp Adiabatic bomb calorimeter. A Carlo Erba 1160 Carbon, Hydrogen and Nitrogen elemental analyser was used for the elemental analysis, oxygen was determined by difference. The Infra-red spectra of the coals were produced using a Nicolet 20SXB Fourier-transform Infra-red spectrometer with the KBr pellet technique. Each spectra was generated using a total of 30 scans per sample.

Petrographic Analyses

All petrographic analyses of the coals were performed on a Leitz MPV3 microscope photometer. Vitrinite reflectance was determined using non-polarised light ($\%R_{\text{Oij}}$ random) on a crushed grain mounted block and based upon 100 measurements. The maceral analyses represent a total of 500 individual counts on grain mounted blocks, using a Swift point-counting device and interpoint and interline distances of $50 \mu\text{m}$. Quantitative fluorescence microscopy on grain mounts of un-crushed coal was achieved using an HBO 100 mercury lamp, an EMI S20 photomultiplier tube (PMT), Ploempak, a Zeiss 'Plan Neofluar' $\times 40$ 0.9n.a. triple-immersion objective (using water), a masked uranyl glass standard and the filter block combinations Tu and I2 (BP 450-490, RKP 510, LP 515). Fluorescence intensity measurements were conducted at 650 nm using a $20 \mu\text{m}$ measuring spot and the I2 filter block combination. A black cavity cell was used to compensate for parasitic reflections and for zeroing the photometer and calibration of the photometer was achieved using an uranyl glass in which the V.D.U. was set to read 100% [8]. Fluorescence intensity measurements scanned across coal particle surfaces was accomplished using an EMI S20 PMT supplemented by a Hamamatsu R446 PMT, which was attached via the camera tube on the microscope trinocular head. The EMI S20 PMT was used for the measurements conducted at 650 nm and the HTV R446 PMT was used for measurements conducted at 546 nm, thereby enabling simultaneous measurements at both wavelengths on the same field-of-view. The interpoint distance of $20 \mu\text{m}$ was achieved using a stepping stage set, with a procedure that involved examining the field-of-view using the Tu filter block, focussing, measuring the reflectance at 546 nm ($\%R_{\text{water}}$, $n = 1.3$ @ 23°C) using the stabilised tungsten lamp, switching over to the I2 filter block and opening the synchro-compur shutter, positioned in front of the mercury lamp, for the duration of the measurement (2 sec) at

I₆₅₀. A new measuring area was then selected using the stepping stage and the process repeated. Chars were produced from the coals (38 to 75 μm size fraction) in an Entrained Flow Reactor [EFR] (Figure 1.) in N_2 at $1273 \pm 5\text{K}$, consisting of a reaction tube of 1.66m length using a gas flow rate of 38 l min^{-1} , to give laminar flow conditions and a residence time of 1 second. Char morphology was analysed in terms of type (from Cenospheres, through Network, to Solid types), depending upon the extent of vesiculation and the porosity of the char, using a Swift point-counter and the Leitz MPV3. The anisotropy of the char types was also recorded using a light microscope (x800 overall magnification) and a Swift point-counter. The internal porosity of each char was derived by Image Analysis using transmitted light on thin sections (5 μm thick) of epoxy mounted char.

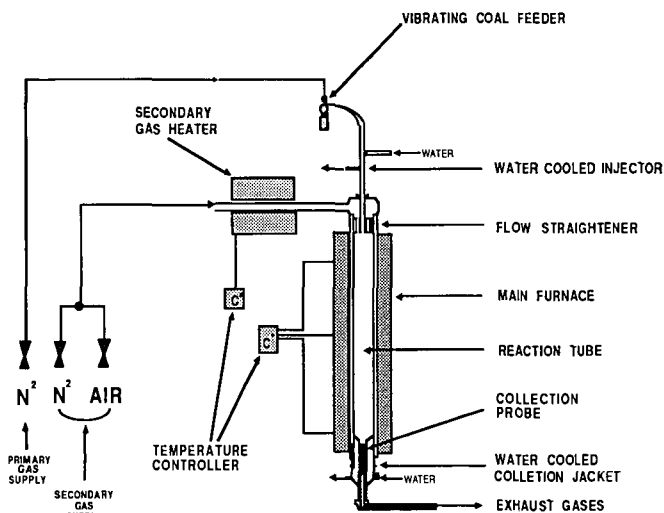


Figure 1. A schematic diagram of the EFR apparatus used in this study.

RESULTS and DISCUSSION

Proximate Analyses

The proximate analyses of the oxidised coals show an initial rapid loss in their volatile matter content, as demonstrated in Figures 2 and 3, with a gradual decrease in the rate of loss as the duration of oxidation increased. For all coals, the rate of volatile matter loss is greater in the artificially oxidised series of coals than for the naturally oxidised coals over a similar period of time, although, in the case of the 88/024 weathered coal series the volatile matter content loss is less than coal series 88/025 and 88/026 over the same period of time reflecting the influence of rank. Despite initial differences in volatile matter content, reflecting the differences in petrographic composition (Table 1.), weathered coals from the 88/025 and 88/026 series attain similar values after 19 weeks and decrease by the same amount over the two successive sampling points.

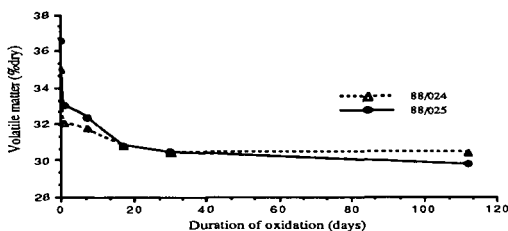


Figure 2. Volatile matter yield and artificial oxidation (air/100°C)

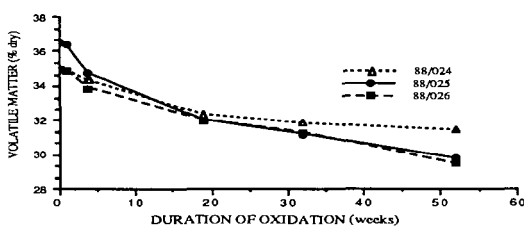


Figure 3. Volatile matter yields and natural oxidation (weathering)

7

These observed trends are augmented by a similar decrease in elemental hydrogen and elemental carbon in preference to oxygen and by a decrease in the calorific content of the coal, as noted previously in a study discussed by Axelson *et al* [6].

Infra-red Analysis and Functional Groups

Infra-red investigations suggest that the main processes taking place involve the progressive removal of aliphatic hydrocarbons and the inclusion of oxygen bearing functionalities within the molecular structure of the coal. The removal of aliphatic hydrocarbons, such as CH_2 and CH_3 , is indicated by a decrease in the absorption bands at 2920, 2850 and 1435 cm^{-1} and is accompanied by the development of absorption bands at 1620-1700 cm^{-1} (ketones), 1690-1718 cm^{-1} (carbonyls in acids), 1765 cm^{-1} (esters) and 1843 cm^{-1} (anhydrides) [9,10]. The development of ring-bound, conjugated, oxygen bearing functionalities is supported in this study by quantitative fluorescence microscopy.

Petrographic analysis of the coals

The vitrinite reflectance values (Figure 4.) increase to approximately 20 to 25% in the artificially oxidised coal series above those values derived from the fresh coals after a period of three months although the reflectance values determined upon the weathered coals decrease over the same period of time. This concurs with the work reported by Puttnam *et al* [4]. The reflectance values determined in this study on oxidised and weathered coals represent measurements on crushed particles of varying size ($>212\mu\text{m}$) embedded within the grain mounted block. The findings within this study relating to the trends outlined for the artificially

oxidised coals concur with those of Prado [11] i.e. that the reflectance varies across the surface of a particle. Both Prado [11] and Cronauer *et al* [12] comment on the absence of visible oxidation rims on low temperature

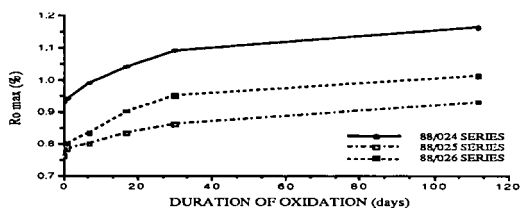


Figure 4. Vitrinite reflectance variation due to artificial oxidation (air/100°C)

artificially oxidised coals when using plain polarised light. Cronauer *et al* [12], artificially oxidising coals under similar conditions to those reported here, considered the kinetics of low temperature oxidation to be diffusion controlled but failed to detect the presence of oxidation rims. They were, therefore, unable to verify their reaction concept. However, in this study, when observing the present series of low temperature artificially oxidised vitrinite coal particles in fluorescent mode, rims of low fluorescence activity (quenched fluorescence) as a direct consequence of oxidation for periods of up to one week, are clearly visible. Therefore, the development of conjugated oxygen bearing groups is supported by the observed quenching of fluorescence in oxidised coals. Ring-bound ketones, for example, have $\pi \rightarrow \pi^*$ and $n \rightarrow \pi^*$ absorptancies at 245 nm and 435 nm. The bond between the ketone and the aromatic group is associated with the $\pi \rightarrow \pi^*$ transition, whereas ketones give rise to the $n \rightarrow \pi^*$ transition. The electronic transitions of oxygen bearing groups increase in both wavelength and intensity with an increasing degree of conjugation. Fluorescence intensity measurements conducted at 650 nm across the polished surface of vitrinite particles (Figure 5) would appear to verify the oxidation kinetics postulated by Cronauer *et al* [12], that the reaction appears to be predominantly diffusional at 100°C and under similar conditions. The rims of quenched fluorescence widen as the period of

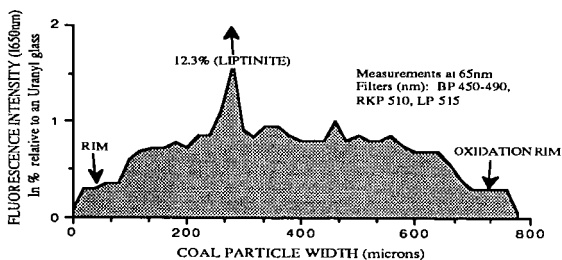


Figure 5. The measured fluorescence intensity across the surface of an oxidised particle of coal (100°C/ air, one day).

artificial low temperature oxidation increases, until eventually no measurable, or visible, fluorescence remains. However, in the case of the weathered coals no well defined oxidation rim exists in the vitrinite particles. Instead the fluorescence intensity diminishes gradually across the particle surface which would suggest that, under the conditions of weathering used in this study, the reactions are probably due to a combination of chemical control and diffusion.

Char morphology

The effects of low-temperature artificial oxidation upon the morphology of chars produced in the EFR are well illustrated by the coal series 88/024 (Figure 6) and the oxidised coal 88/025 series (Figure 7). Both unoxidised coals 88/024 and 88/025 are vitrinite rich (see Table 1.) and are of sufficient rank to produce a predominance of cenospheric char forms [Plate 1.].

Proportion of
anisotropic char 92.4% 34.2% 2.2% 0% 0% 0%

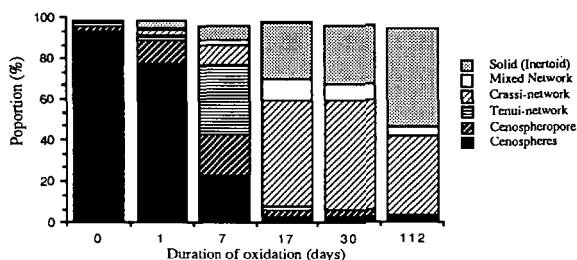


Figure 6. EFR chars and the artificial oxidation of coal 88/024

Proportion of
anisotropic char 46.2% 27.8% 1.4% 0.8% 0% 0%

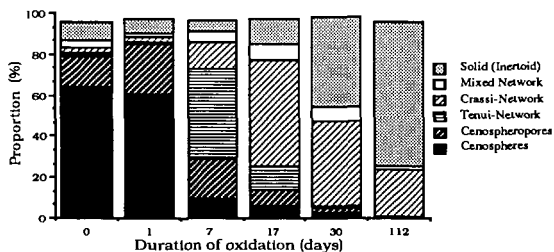


Figure 7. EFR chars and the artificial oxidation of coal 88/025

The proportion of cenospheres produced during pyrolysis from the unoxidised coals and the percentage of char exhibiting visible anisotropy follows the rank dependence postulated previously [13]. However, the effects of artificial oxidation are most severe on the higher rank series 88/024. The decrease in the proportion of anisotropic char, from an original value of 92.4% down to 34.2% after oxidation at 100°C for one day, is notable. This is followed by a virtual elimination of all visible anisotropy in the chars after oxidation for one week. Furthermore, the systematic replacement of cenospheres by isotropic chars of a less-vesiculated nature, i.e. the tenui-network chars [Plate 2.], until the predominant char type is a dense and solid *inertoid* char type of low porosity [Plate 3.] as oxidation time increases (Figures 6 and 7) is a clear indication of the loss of thermoplastic properties during pyrolysis.

Deshpande *et al* [14] discuss the nature of molecular cross-linking and volatile evolution during the pyrolysis of coal in relation to the rank of the feedstock and the decomposition of carboxyl groups during pyrolysis. During the slow pyrolysis of a lignite ($0.5^{\circ}\text{C s}^{-1}$), cross-linking starts to develop prior to the evolution of tar. At higher heating rates ($2.0 \times 10^4 \text{ }^{\circ}\text{C s}^{-1}$), cross-linking occurs simultaneously with tar evolution. Similarly, the thermoplasticity of a bituminous coal has been attributed to both the presence of cross-links in the macromolecular framework of the coal (vitrinite) and the behaviour of the "mobile phase" during pyrolysis [15]. Upon heating, the macromolecule decomposes and the coal exhibits visco-elastic properties allowing the aromatic units to slide over one another. The volatile matter, which is generated within the macromolecular framework, expands causing the viscous mass (proto-char) to expand during the simultaneous expulsion of gaseous material. The result is the production of a char, the morphology of which is largely dependent, according to the model of Spiro, upon the behaviour of the mobile phase during char formation.

Char formation cannot be readily explained by visco-properties alone. The formation of radicals is also significant during pyrolysis. The formation of radicals, which are highly reactive. Under the operating conditions of the E.F.R., and their probable stabilisation and transformation into volatile species, is possibly achieved primarily by hydrogen addition. The formation of the char particle is followed by the polymerisation and condensation reactions that occur during the recombination of non-volatile radical components. Therefore, the depletion of donatable hydrogen species through the oxidative replacement of reactive benzylic CH_3 or CH_2 groups possibly leads to a greater number of non-stable oxygen bearing radical components during pyrolysis. Solomon and Haublen [16] formulated a 'functional group model', in which coal pyrolysis is regarded as a depolymerisation process that operates parallel to the decomposition of functional groups, in which the pyrolysis products compete for hydrogen-capping moieties for stabilisation. According to this model, the type and number of functional groups therefore control the kinetics and mechanisms that operate during pyrolysis.

There is some confusion in the literature [17] regarding the effects of oxidation on vitrinite reflectance. Such confusion exists because the oxidation of coal is dependent upon particle size and the temperature under which the gas-solid reaction takes place. In oxidative techniques that employ high temperatures, there is a 'reaction front', visible as a rim (heterogeneous gas-solid reaction), under low temperature conditions, such as natural weathering, there is no discernible reaction front and the oxygen appears to react progressively throughout the particle (homogeneous gas-solid reaction). Measurements conducted, wittingly or otherwise, on the central area of the particle *beyond the gas-solid reaction front* will lead to variations in reflectivity not necessarily due to the chemical process of oxidation.

Bulk analytical techniques, such as proximate analysis, do not adequately predict the behaviour of oxidised pulverised fuel during pyrolysis or combustion. The techniques discussed above indicate values associated with coals of higher rank, although the behaviour of the oxidised coal during pyrolysis is more akin to low rank coals or coals containing a high proportion of the maceral inertinite. Therefore, careful monitoring of properties is necessary when stockpiling coal and the utilisation of petrographic techniques, such as fluorescence microscopy and the safran-o staining technique [6] will help to discriminate between oxidised and unoxidised coals.

CONCLUSIONS

The progressive oxidation of coal feedstock severely alters the nature and morphology of the char produced during EFR pyrolysis. More specifically:

1. Artificial oxidation of the coal leads to a reduction in the porosity of the char, through a decrease in the extent of devolatilisation and a probable increase in the extent of cross-linking. Furthermore, there is a decrease in the anisotropy of the char as a result of oxidation.
2. The effect of weathering is similar to those witnessed by artificially oxidised coals, although the time required for comparable changes is much greater.
3. Existing coal characterisation techniques do not adequately assess the effect or extent of oxidation and some techniques, such as vitrinite reflectance show variations not necessarily due to oxidation, but more to the experimental conditions (temperature) employed.
4. Petrographic techniques, such as fluoremetry, are sensitive to the type and extent of oxidation and therefore represent a useful means of characterising oxidised coal feedstock.

References:

- [1] Neavel, R.C., in 'Coal Science', (Eds. M.L. Gorbaty, J.W. Larsen, and I. Wender) 1982 2 Academic Press, New York. 1
- [2] Larsen, J.W., Lee, D., Schmidt, T., and Grint, A., 1986 Fuel **65** 595
- [3] Pis, J.J., Cagigas, A., Simon, P., and Lorenzana, J.J., 1988 Fuel Proc. Technol. **20** 307
- [4] Puttmann, W., Steffens, K. and Kalkreuth, W. 1987 Int. Conf. on Coal Science (Moulijn J.A., Nater, K.A., Chermin, H.A.G. Eds.) Elsevier 411
- [5] Nandi, B.N., Brown, T.D. and Lee, G.K., 1977 Fuel **56** 125
- [6] Axelson, D.E., Mikula, R.J. and Munoz, V.A. 1987 Int. Conf. on Coal Science (Moulijn J.A., Nater, K.A., Chermin, H.A.G. Eds.) Elsevier 419
- [7] Ottaway, M. 1982 Fuel **61** 713
- [8] Diesel, C.F.K and McHugh, E.A., 1986 Gluckauf-Forschungshefte **47** 60
- [9] Painter, P.C., Snyder, R.W., Starsinic, M. and Coleman, M.M. 1981 Applied. Spectroscopy **35** 375
- [10] Calemma, V., Rausa, R., Margarit, C.N. and Giradi, B. 1988 Fuel **67** 764
- [11] Prado, J.G. 1977 J. of Microscopy **100** 85
- [12] Cronauer, D.C., Ruberto, R.G., Jenkins, R.G., Davis, A., Painter, P.C., Hoover, D.S., Starsinic, M.E. and Schlyer, D. 1983 Fuel **62** 1125
- [13] Bend, S.L., Edwards, J.A.S. and Marsh, H., 1988 'Carbon '88' (McEnaney, B. and Mays, T.J. Eds.) IOP Bristol 594
- [14] Deshpande, C.V., Solomon, P.R. and Serio, M.A. 1988 ACS Div. of Fuel Chem. **33** No 2 310
- [15] Spiro, C.L. in 'Space filling models for coal: A Molecular Description of Coal Plasticity' 1981 Internal Report. General Electric. Schenectady, New York
- [16] Solomon, P.R. and Hamblen, D.G. in 'Chemistry of Coal Conversion' (Schlossberg R.H. Ed) 1985 Plenum Press. New York 121
- [17] Stach, E., Mackowsky, M.-Th., Teichmüller, M., Taylor, G.H., Chandra, D. and Teichmüller, R. 1982 Textbook of Coal Petrology. 2nd Rev. Ed Gebrüder Borntraeger Berlin 535

ACKNOWLEDGEMENTS

S.L.B. thanks J. Pearson of British Coal for the samples of fresh coal.

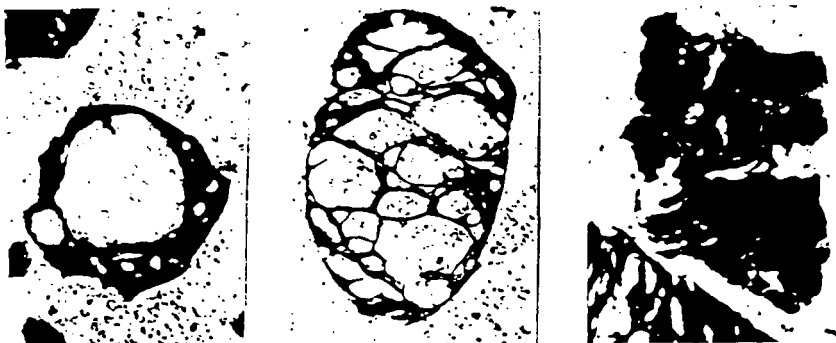


Plate 1.

Plate 2.

20µm

Plate 3.

Transmitted light photomicrographs taken through thin sections of epoxy mounted char, showing the cross-sectional morphology and internal porosity due to variations in vasculation and devolatilisation. Plate 1. shows a Crassinensphere (thick-walled cenosphere): 68% porosity. Plate 2. shows a Tenuinetwork char: 65% porosity. Plate 3. shows a Crassinetwork char (bottom left): 43% porosity; and an Inertoid, in which no vasculation pores are visible although shrinkage cracks are visible: 15% porosity